Research article

Chunlei Sun, Wenhao Wu, Yu Yu*, Guanyu Chen, Xinliang Zhang, Xia Chen, David J. Thomson and Graham T. Reed

De-multiplexing free on-chip low-loss multimode switch enabling reconfigurable inter-mode and inter-path routing

https://doi.org/10.1515/nanoph-2018-0053
Received May 1, 2018; revised July 10, 2018; accepted July 24, 2018

Abstract: Switching and routing are critical functionalities for a reconfigurable bandwidth-dense optical network, and great efforts had been made to accommodate mode-division multiplexing technology. Although the reconfigurable routing for spatial-mode groups between different optical paths was realized recently, a demultiplexing-switching-multiplexing process is necessary. Here we present a simplified and compact on-chip 2×2 multimode switch that can be easily upgradable to a larger scale. Fully and reconfigurable routing between not only optical paths but also spatial modes is achieved. To obtain a low loss multimode processing, a novel structure free from demultiplexing and re-multiplexing operations is adopted. The switch enables minimum and maximum insertion losses of 0.3 and 1.2 dB, with a compact footprint of 433 μm × 433 μm and low crosstalk of <–16.6 dB for all channels. It is further extended to two types of 4×4 switch fabrics with cross-bar and ring-bus architectures, as demonstrations of high-level integration. System characterization with 32 Gb/s high-speed modulated signals is also carried out, reaching up to 256 Gb/s aggregate throughput. These results verify a general solution of 2×2 multimode switch for reconfigurable inter-mode and inter-path routing applicable in large-scale and high-density multimode optical network.

Keywords: mode-division multiplexing; optical interconnect; optical switching; silicon photonics.

***Corresponding author: Yu Yu,** Wuhan National Laboratory for Optoelectronics, Huazhong University of Science and Technology, 1037 Luoyu Road, Wuhan 430074, China, e-mail: yuyu@mail.hust.edu.cn.
http://orcid.org/0000-0002-8421-6794
Chunlei Sun: Wuhan National Laboratory for Optoelectronics and School of Optical and Electrical Information, Huazhong University of Science and Technology, Wuhan 430074, China; and Optoelectronics Research Centre, University of Southampton, University Road, Southampton, Hampshire SO17 1BJ, UK
Wenhao Wu, Guanyu Chen and Xinliang Zhang: Wuhan National Laboratory for Optoelectronics and School of Optical and Electrical Information, Huazhong University of Science and Technology, Wuhan 430074, China
Xia Chen, David J. Thomson and Graham T. Reed: Optoelectronics Research Centre, University of Southampton, University Road, Southampton, Hampshire SO17 1BJ, UK

1 Introduction

Optical interconnects with broad bandwidth, low power dissipation and multiplexing compatibility have become a disruptive technology with a variety of applications such as intra-chip interconnects, short-reach communications in high-performance computers and datacenters and long-haul communication networks [1, 2]. Benefitting from diverse multiplexing techniques, great strides have been achieved in optical interconnects for single-mode optical systems. Among these techniques, the wavelength-division multiplexing (WDM) involving numerous wavelengths in a shared channel has been one of the most successful in the past decades [3–9]. To satisfy the exponentially increasing data demand, an emerging technique, mode-division multiplexing (MDM), is becoming more and more attractive as multiple spatial modes share a single-wavelength link to further improve the communication capacity [10, 11]. It is of great interest to fulfill high-bandwidth-density interconnects by combining these two techniques to construct a hybrid multiplexing system [12].

On the other hand, reconfigurable photonic integrated devices, which allow dynamic data rearrangement and increase flexibility as well as throughput, are the key components of optical networks. A compact and low-loss switching device is promising for data-hungry and power-consumption-sensitive applications such as optically interconnected processors and memories [13, 14]. Previously, many researches were focused on single-mode

system, and various high-performance single-mode switch elements and fabrics with high-port count were achieved [15–27]. Recently, switches for multimode signals were proposed and demonstrated [28–34]. While more ports and larger scale were developed, multiple dimensions were also introduced with reconfigurable and more powerful routing capability. In [28], Wu et al. realized a 1×3 switch processing three modes. Add-drop functionality was achieved in the 1×1 multimode switch for four-mode channels [29, 30]. The 1×2 multimode switches were demonstrated by combining WDM or polarization-division multiplexing with MDM [31, 32]. Compared with a single-input-port switch, a double-input-port case is more efficient since it can tackle two optical links. In [33], a 2×2 mode switch that routed four modes was demonstrated. The aforementioned switches are limited to path routing, and the signal is carried on the fixed mode. Recently, Yang et al. proposed a 2×2 switch. Reconfigurable global mode routing (not only path routing, but also mode routing among different spatial mode channels) was fulfilled to extend the freedom degree of reconfigurable routing [34]. The approach is de-multiplexing all the input multimode signals to fundamental modes and processing them individually by utilizing single-mode elements. Then the fundamental modes can be multiplexed back to the target output modes. Nevertheless, a large insertion loss (>10 dB), which is mainly attributed to the multiplexer (MUX)/demultiplexer (DEMUX) and complicated layout, was induced [34]. Such a demultiplexing-processing-multiplexing procedure results in a quite complicated configuration and puts forward higher requirements for the mode (DE)MUX performance. In contrast, previous works for one-stop multimode processing, which can be free from demultiplexing and multiplexing operations, have been realized and are promising for the 2×2 multimode switch [35–37].

Multiple 1×2 or 2×2 switching elements can be potentially cascaded with different network architectures to obtain higher-port-count switch fabrics and bandwidth-dense interconnects. The choice of switching elements determines the footprint, crosstalk, switching loss and the switch fabric architecture. In this paper, we present a compact and low loss 2×2 multimode switch that is easily scalable to high-port-count switch fabrics. It consists of a pair of 1×1 Mach-Zehnder interferometer (MZIs) multimode switches and a pair of micro-ring (MR) 2×2 single-mode switches. Reconfigurable inter-mode plus inter-path routing for fully flexible on-chip optical networks can be achieved. The input multiplexed signals can be processed simultaneously without a complicated demultiplexing-processing-multiplexing procedure. It is convenient to extend the design to support more mode channels by adopting a multi-arm MZI structure [38] and cascaded symmetric Y-junctions in a plane. The proposed switch is experimentally demonstrated with a low insertion loss of <1.2 dB and a low crosstalk of <–16.6 dB for all channels and switching configurations. We also demonstrate two representative types of 4×4 switch fabrics with cross-bar and ring-bus architectures by assembling multiple proposed switch elements. These two types of switch fabrics are optimized for different functionalities. The first realizes strictly non-blocking and almost path-independent insertion loss (PILOSS), while the latter one is non-blocking and can make full use of the optical paths. System characterization with 32 Gb/s high-speed non-return-to-zero on-off keying (NRZ-OOK) signals is carried out, reaching up to 256 Gb/s of aggregate throughout.

2 Switch design

Figure 1A illustrates the schematic of a high-port-count multimode switch fabric. Low loss waveguide crossings constitute the backbone of the optical network. To enable WDM grid compatibility, MRs are introduced to change the light propagation direction. Multiple WDM channels can be supported when the free-spectral range (FSR) is set as the wavelength spacing. Each input or output waveguide supports two modes. The numeric strings with red and green colors represent the signals carried on the fundamental transverse electric mode (TE_0) and first-order transverse electric mode (TE_1), respectively, as shown in Figure 1A. The input signals can be optionally converted to the desired output modes. Figure 1B shows the fundamental 2×2 multimode switch element, which is elaborately designed with a pair of MZI-based 1×1 multimode switches intersecting with each other and a pair of MR-based 2×2 single-mode switches. Two symmetric Y-junctions are employed to construct the MZI structure, and they act as power splitter and combiner for both TE_0 and TE_1 modes. For the splitter, the input TE_0 is equally split into two parts with zero phase difference, while TE_1 is split into two TE_0 modes with π phase difference. At the combiner, the two TE_0 modes are then combined back into TE_0 or TE_1 mode, depending on the phase difference [35]. A waveguide crossing is positioned close to a MR, forming a 2×2 single-mode switch. The MR heater H2 and MZI heaters H1 and H3 are utilized for reconfigurable control, performing two possible states: OFF and ON. In the OFF state, the resonance wavelengths of the two MRs deviate from the operating wavelength with half FSR to minimize the crosstalk, and thus no power couples into the MR and

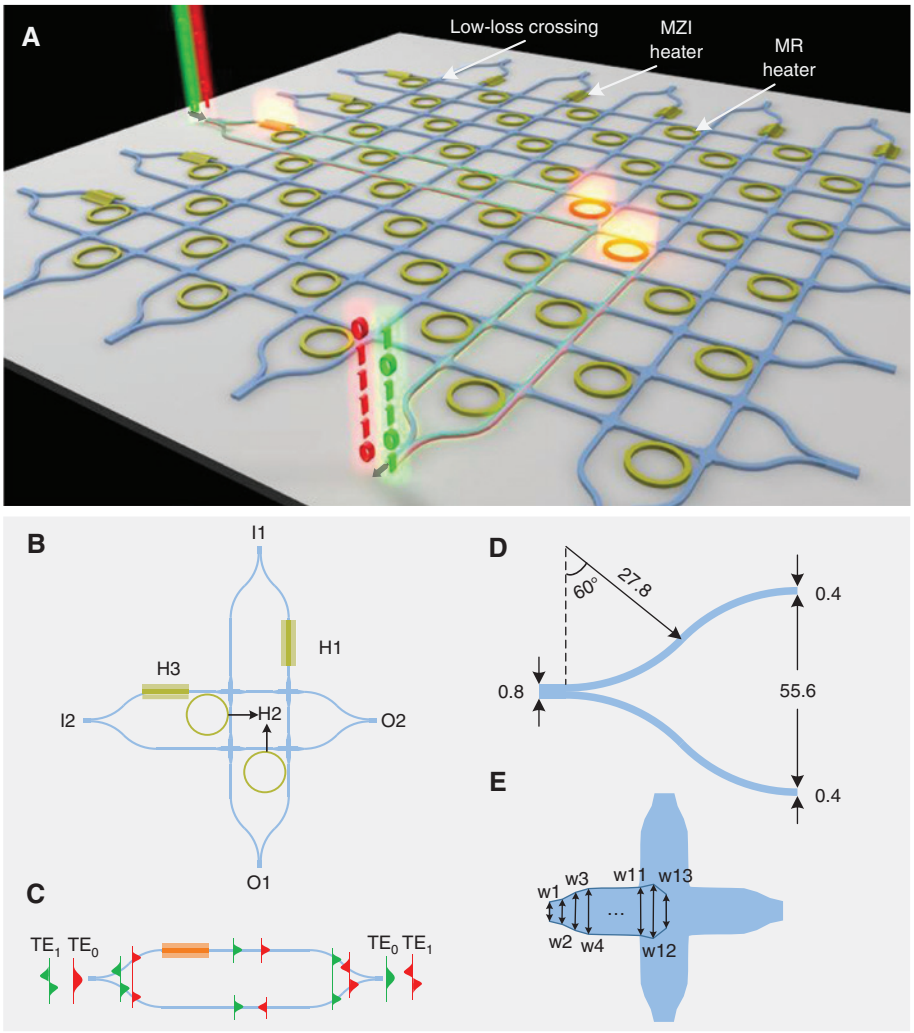

Figure 1: The proposed integrated multimode switch.
(A) Schematic of high-port-count multimode switch fabric. The numeric strings with red and green colors stand for the signals carried on different modes. The signal can be selectively guided to the desired output port as the desired mode. (B) A 2×2 multimode switch element consisting of two Mach-Zehnder interferometer (MZI) based 1×1 multimode switches orthogonally intersecting with each other and two micro-ring (MR) based 2×2 single-mode switches. The thermal heaters are used for reconfigurable control. (C) MZI-based 1×1 multimode switch. The TE_0 and TE_1 modes exchange with each other in the ON state. Schematic views of (D) the symmetric Y-junction and (E) waveguide crossing.

the signal is guided to the through port uninterruptedly. In the ON state, the light is coupled into the MRs as the resonance wavelengths are shifted to align with the operating wavelength, making a 90° direction change and outputting the light from the drop port. These two MRs always work with same switching states and resonance wavelengths. Note that the MR-based switch here is different from the traditional work in [24], where each MR serves as a 1×2 single-mode switch, and the resonance wavelengths of the MRs should be different to realize wavelength multiplexing or de-multiplexing. For the heaters H1 and H3, by controlling the phase difference between the two MZI arms, the data information carried on the two input modes can be exchanged or remain the same. In the OFF state, no phase difference is introduced; thus, the data are carried on the original modes. In the ON state, a π phase difference is introduced; thus, these two modes are exchanged with each other, as shown in Figure 1C. Therefore, the MZI-based 1×1 multimode switch functions equivalently as a structure consisting of a mode MUX, a DEMUX and a 2×2 single-mode switch, avoiding the performance degradation due to unnecessary (de)multiplexing.

For clarity of presentation, we only choose the TE_0 mode injected from port I2 as an example to illustrate the reconfigurable inter-mode and inter-path routing. In this regard, the output results are only determined by the states of the heaters H2 and H3, which are independent of heater H1 that only impacts the light injected from

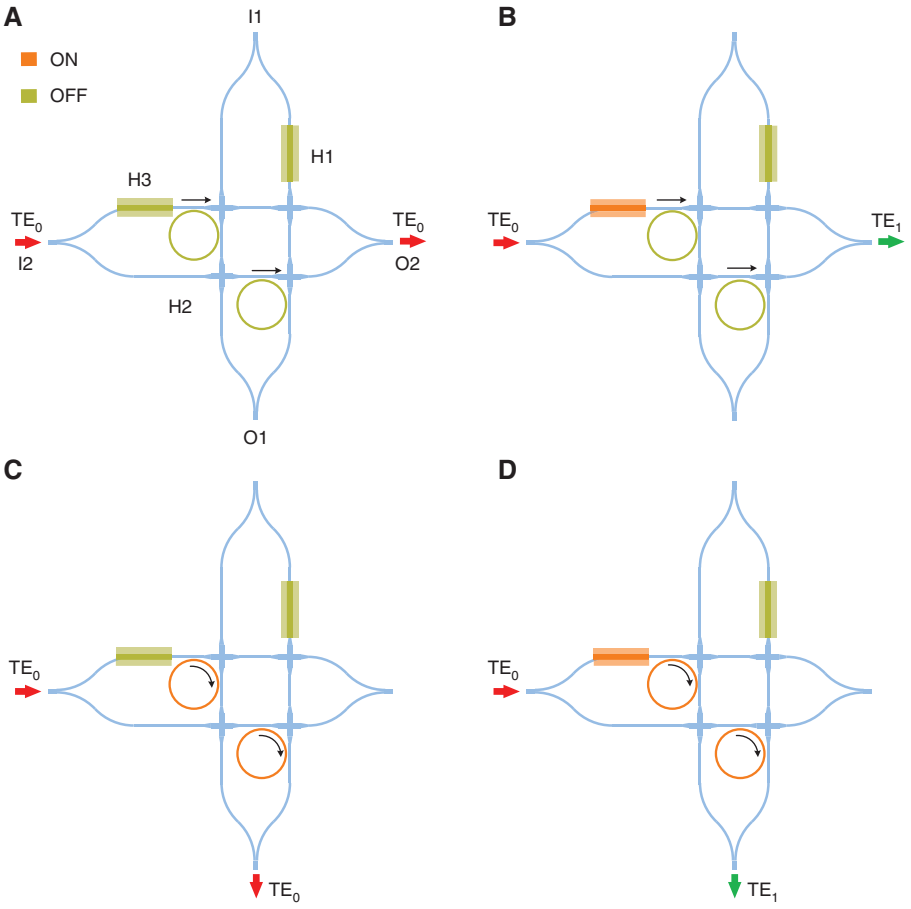

Figure 2: (A–D) Four different routing states for the TE_0 mode launched into port I2 for four switching configurations. The orange stands for the ON state, while the gold stands for the OFF state.

port I1. The output results for all the permutations and combination states of H2 and H3 are shown in Figure 2. In the OFF states for both heaters H2 and H3, the input light propagates straight to port O2 with the output mode unchanged (Figure 2A). When the heater H3 is switched to the ON state, the input signal on TE_0 mode still travels to O2 while it transforms into the TE_1 mode at the output (Figure 2B). When the heaters H2 and H3 are in the ON and OFF states, respectively, the light turns to port O1 as the TE_0 mode (Figure 2C). For the ON states of both heaters H2 and H3, the light propagates to port O1 as the TE_1 mode (Figure 2D). In these scenarios, there are four different output results for the single input case. The MZI heater H3 is responsible for inter-mode routing, while the MR heater H2 determines the inter-path routing. The situation is similar when the TE_0 mode is injected from port I1. Therefore, the 2×2 multimode switch element has a complete set of eight routing states corresponding to three individual heaters, as summarized in Table 1. The signals 1 and 2 carried on the TE_0 and TE_1 modes are injected from I1, while signals 3 and 4 carried on the TE_0 and TE_1 mode are injected from I2. When the switch element is extended to M-modes, there will be a total of 2×(M!)2 routing states. For an N×N M-mode strictly non-blocking switch fabric, in which the paths from any input

Table 1: Complete set of routing states of proposed multimode switch.

I1		I2		States	O1		O2	
TE_0	TE_1	TE_0	TE_1	(H1, H2, H3)	TE_0	TE_1	TE_0	TE_1
1	2	3	4	(F, F, F)	1	2	3	4
				(F, F, O)	1	2	4	3
				(F, O, F)	3	4	1	2
				(F, O, O)	3	4	2	1
				(O, F, F)	2	1	3	4
				(O, F, O)	2	1	4	3
				(O, O, F)	4	3	1	2
				(O, O, O)	4	3	2	1

The numbers 1, 2, 3 and 4 refer to different signals carried on the different mode. The letter O stands for the ON state, while F stands for the OFF state.

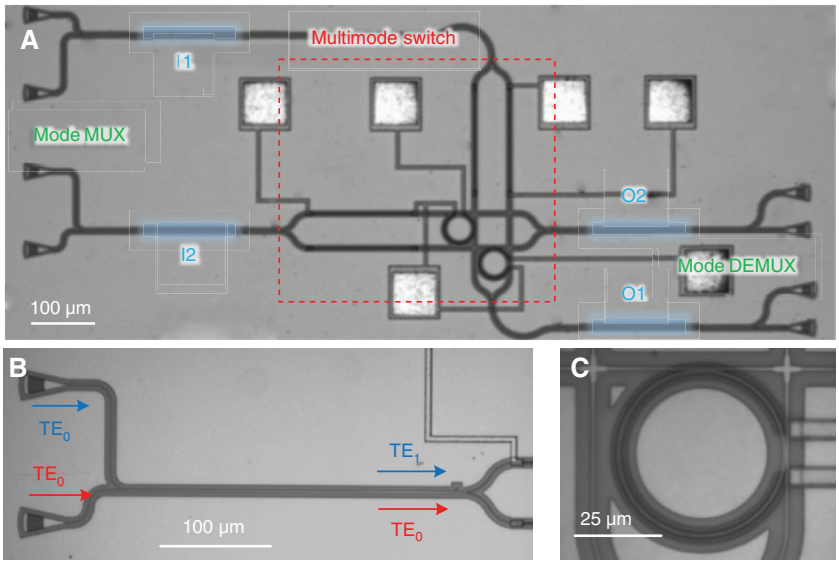

Figure 3: Fabricated multimode switch.
(A) Microscope image of the fabricated device consisting of the proposed multimode switch and mode (DE)MUXs. The region highlighted with the red dashed line shows the multimode switch. The areas highlighted in blue show the input/output multimode waveguides. Zoom-in images of (B) the mode MUX and (C) micro-ring resonator.

port to any output port can be established at the same time as the state of the switch elements on a given path is independent to all the others [18, 24, 39, 40], there are N! × (M!)N routing states in total.

The proposed switch is designed on the silicon-on-insulator platform with 220 nm thick top silicon layer. For the Y-junction shown in Figure 1D, the widths of the branch and stem parts are 0.4 and 0.8 μm, respectively. The branch is composed of two mirrored S-bends with radius and bend angle of 27.8 μm and 60°. Figure 1E shows the schematic view of the waveguide crossing composed of four multimode waveguides, which is divided into 12 segments with equal length. The particle swarm optimization method is utilized to optimize the geometry (w1-w13). The optimized parameters w1-w13 are 0.5, 0.6, 0.95, 1.32, 1.44, 1.46, 1.466, 1.52, 1.58, 1.62, 1.76, 2.15 and 0.5 μm, respectively. The waveguide crossing was reported in a previous paper with very low insertion loss of <0.03 dB and low crosstalk of <–37 dB [41]. The coupling gap and radii of the MR are chosen as 0.2 and 24 μm, so as to obtain a broad bandwidth and a high extinction ratio for high-speed transmission.

3 Results

To form the waveguide structure, 248 nm deep ultraviolet lithography and inductively coupled plasma etching were employed. Metal titanium was deposited on the top of the MRs and the arms of MZIs, serving as the heaters for thermal tuning. The SiO_2 cladding is utilized to cover the entire device, forming a buffer layer between the metal heater and waveguide. The microscope image of the fabricated device is shown in Figure 3. Extra mode MUXs based on adiabatic couplers are utilized to implement the multiplexing for input light coupled from an off-chip single-mode transmitter [42], as shown in Figure 3B. The region highlighted with a red dashed line shows the switch with a compact footprint as compact as 433 μm × 433 μm. Figure 3C shows the zoom-in image of MR resonator.

We measure the transmission spectra of the fabricated device over a wavelength range from 1520 to 1570 nm. For clarity, only spectra around 1550.29 and 1568.6 nm when the two modes are launched into port I2 are illustrated in Figure 4A and B. The legend indicates the states of the heaters H2 and H3; e.g. "F-O" refers to the transmission in the OFF state of H2 and ON state of H3. By deducting the loss caused by the grating couplers, mode MUX and DEMUX, the measured minimum and maximum insertion loss are 0.3 and 1.2 dB, respectively. The 3 dB optical bandwidth of the MR is 46.3 GHz, which agrees well with the designed value of 45 GHz. The mode-dependent insertion loss of <1 dB mainly results from the larger propagation loss of the Y-junction for TE_0 mode, since more power of TE_0 locates in the center of the waveguide, inducing a stronger reflection by the inner corner of the symmetric Y-junction. The path-dependent insertion loss is measured to be <0.5 dB, and the inter-path crosstalk and inter-mode crosstalk are <–16.6 dB and <–20 dB for all the cases. The

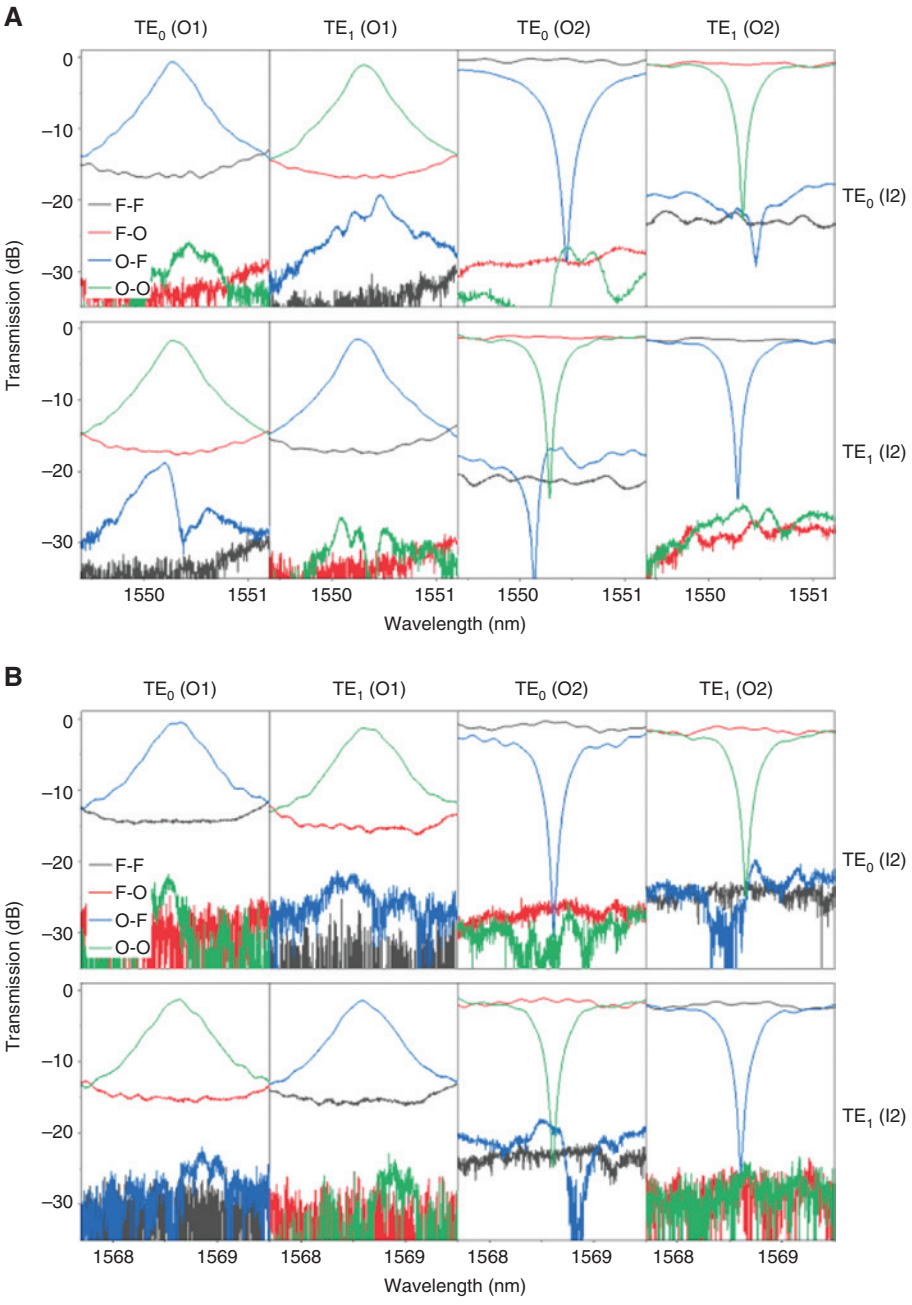

Figure 4: Measured transmission spectra around the wavelengths of (A) 1550.29 nm and (B) 1568.6 nm for all of the permutations and combination states of the heaters H2 and H3 when the TE_0 mode and TE_1 mode are launched into port I2.
The letters in the legend "F-O" refer to the OFF state of heater H2 and the ON state of heater H3, respectively.

major crosstalk comes from the inter-path one which can be further improved by adopting a MR with higher extinction ratio. The thermal instability of MRs can be overcome by implementing a thermal stabilization platform. For the MZI, the heating power and drive voltage are 18 mW and 7.1 V, when switching from OFF to the ON state. For the MR, the power of switching resonance wavelength to half FSR is 17.5 mW, and the voltage is 5.8 V. The thermal tuning structure is quite common and has been extensively applied in literatures, showing a typical switching time around tens of microseconds [43, 44].

In order to achieve a real commercial success, high-level integration by assembling numerous photonic components is the development trend, as it can improve the link price, performance and power dissipation. Thus, a large-scale and high-density integration of the switch fabrics, combining multiple multimode switch elements and making MDM technique more attractive and valuable,

is highly desired. Here, we fabricated two types of switch fabrics with cross-bar and ring-bus architectures based on our proposed elements to verify high-level integration, as shown in Figure 5A and B, respectively. They both consist of four switch elements with eight thermal heaters, and the simplified schematics are given in Figure 5C and D. The area highlighted in red refers to the switch element. The black arrows indicate the light propagation directions. These two types of switch fabrics are optimized for different functionalities. For the cross-bar switch fabric, light is switched (at most) twice through the MR. There is almost no cumulative switching loss, in spite of scaling up to higher port count. The switch fabric is not strictly non-blocking as each input port has different properties, e.g. the light launched into port I1 can be routed to any output port, while the light path between port I2 and port O1 cannot be established physically. There is a total of 384 routing states for a 4×4 strictly non-blocking multimode switch fabric. Excepting the physically unestablished optical paths such as "I2 to O1" and "I3 to O4", there remain 224 routing states. If the ports I3, I4, O1 and O2 are idle and the rest are used, the architecture will be

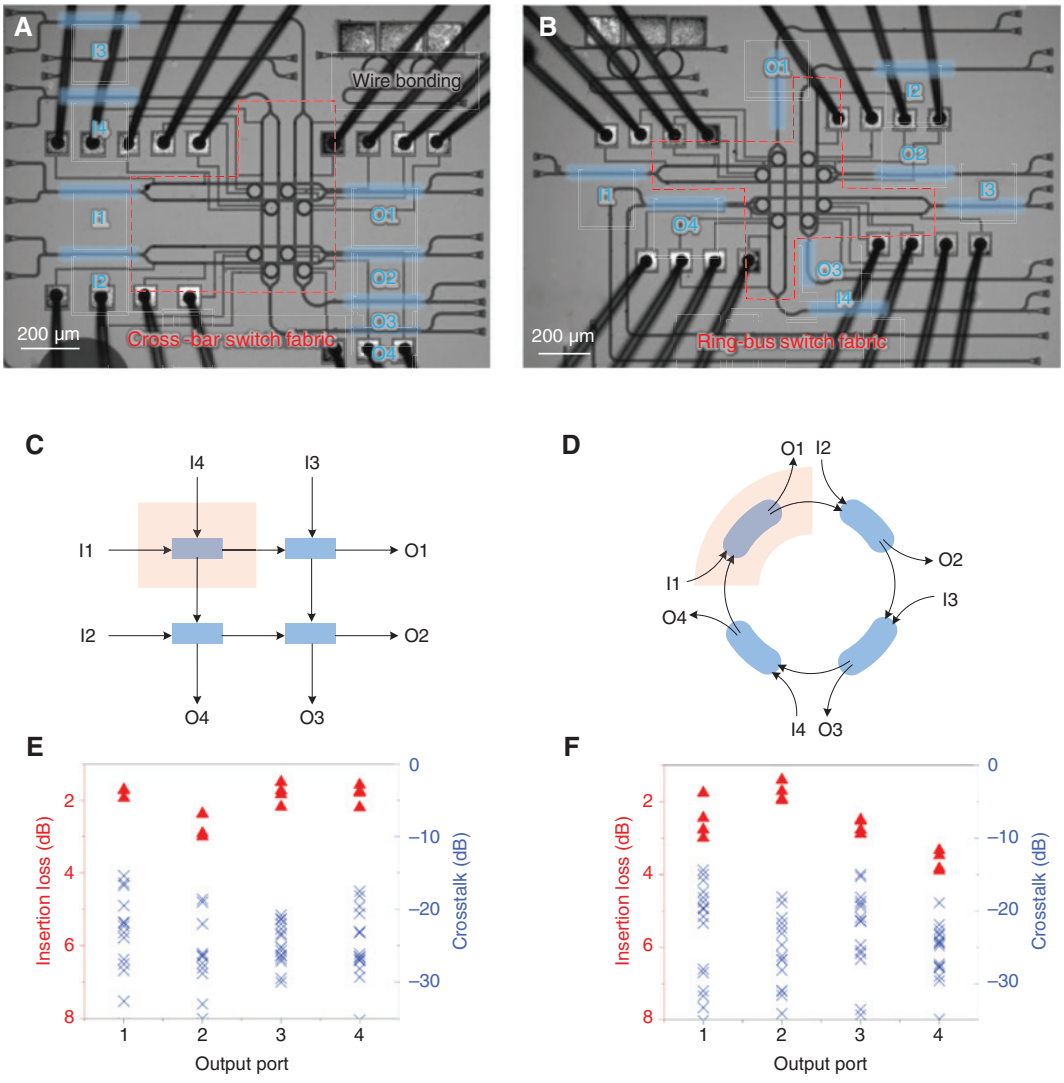

Figure 5: Fabricated multimode switch fabrics.
Microscope images of the two types of 4×4 switch fabric with (A) cross-bar and (B) ring-bus architecture based on the multimode switch elements. The wire bonding technique is used for electrical connection between the on-chip electrode pads and the printed circuit board pads. Simplified schematics of (C) cross-bar and (D) ring-bus switch fabrics. The areas highlighted in red refer to the switch element. The black arrows indicate the light propagation directions. Measured insertion loss and crosstalk at each output port for all the permutations and combination states of the heaters at 1550.29 nm when the light injected from port I1 of both the (E) cross-bar switch fabric and (F) ring-bus switch fabric.

strictly non-blocking. The ring-bus switch fabric has a rotational symmetry structure. Thus, each input port has the same property, and it allows arbitrary access to any output ports. Such a reconfigurable optical switch fabric makes full use of the optical paths. The ring-bus architecture is rearrangeable and non-blocking. For instance, if the optical path "I1-O4" is established, the path "I2-O3" will be blocked. Therefore, it might be necessary to rearrange ongoing transmissions to satisfy a certain connection. There are a total of 192 non-blocking routing states.

These two switch fabrics are fully characterized for all the channels and switching configurations. Both TE_0 and TE_1 modes at 1550.29 nm are injected from port I1 of the cross-bar switch fabric (Figure 5E) and ring-bus switch fabric (Figure 5F). The insertion losses are extracted by subtracting the loss of fiber-chip coupling, mode multiplexing and demultiplexing. For the cross-bar fabric, the insertion loss is 1.5–3.0 dB, and the path-dependent loss is <0.9 dB. Compared to the fundamental switch element, the cross-bar switch fabric has

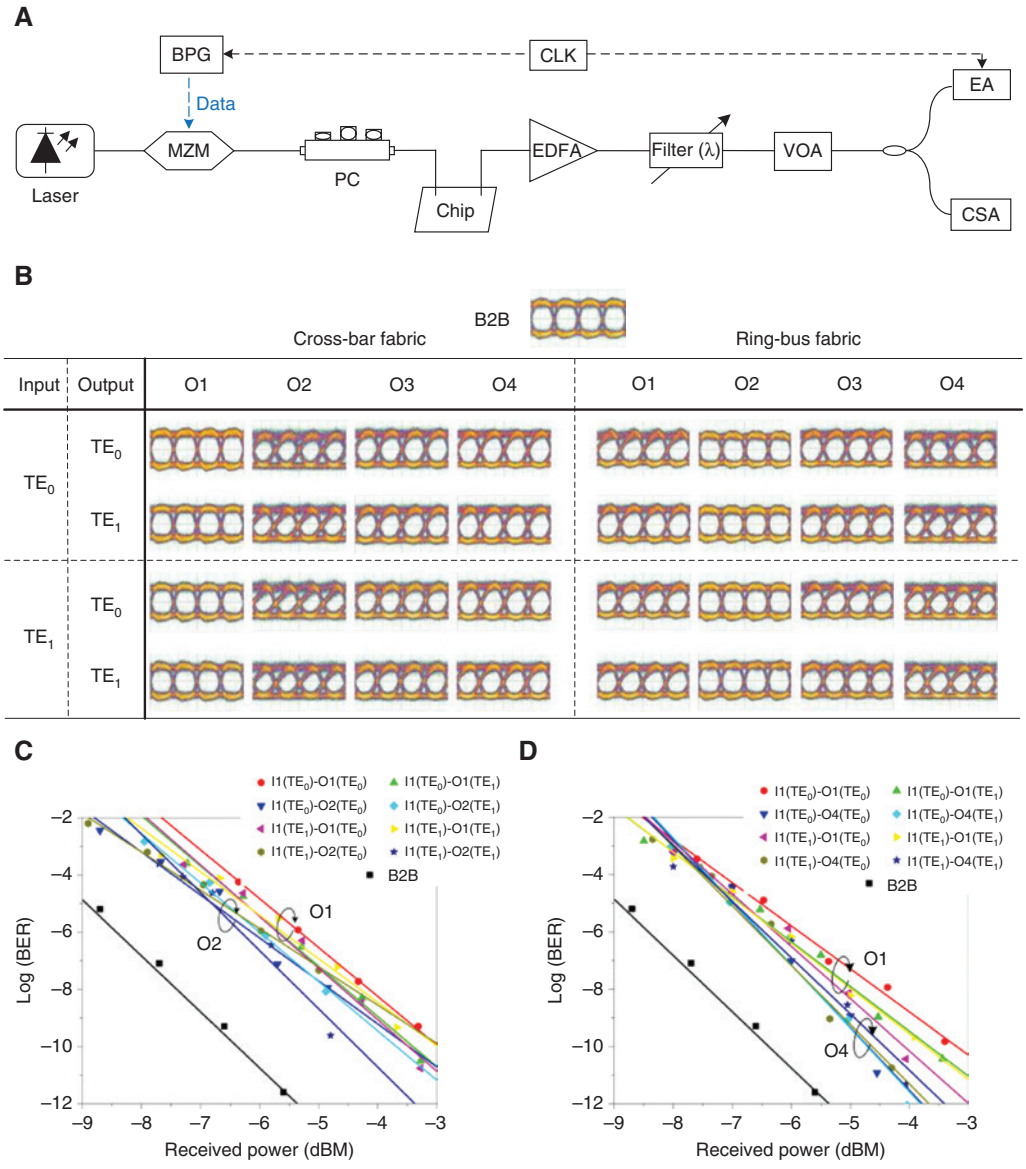

Figure 6: High-speed signal characterization for the two switch fabrics.
(A) High-speed signal testing setup including a tunable laser, a polarization controller (PC), a Mach-Zehnder modulator (MZM), a bit pattern generator (BPG), an Er-doped fiber amplifier (EDFA), a tunable bandpass filter, a variable optical attenuator (VOA), a communications signal analyzer (CSA) and an error analyzer (EA). (B) Measured 32 Gb/s eye diagrams for the B2B case, and each output port at 1550.29 nm when the light injected from port I1 of the cross-bar switch and ring-bus switch fabrics. Bit error rates of (C) optical paths "I1-O1" and "I1-O2" for the cross-bar switch fabric and (D) "I1-O1" and "I1-O4" for the ring-bus switch fabric.

no significant increase in insertion loss. Approximate PILOSS functionality can be realized. For the ring-bus fabric, the insertion loss is 1.3–3.8 dB, and the path-dependent loss is <1.9 dB. The larger path-independent loss is attributed to the cumulative switching loss in the light path. The measured crosstalk for the two fabrics is lower than –15 dB. Note that the I1-O4 path, which includes eight MRs (four MRs in OFF state, the other in ON state) with 3.8 dB insertion loss, is the longest and most complicated path. Within the cumulative switching loss, a non-negligible part comes from the MRs' resonance wavelength misalignment caused by thermal crosstalk. It can be efficiently cut down by adopting a larger gap or by using a deeply etched isolation trench between these MRs [17]. Compared with the reported 2×2 four-mode switch with loss of 10–14.9 dB [32], our 4×4 dual-mode switch fabrics achieve a much smaller insertion loss (3.8 dB) with similar scale, which are readily applied in high-port-count optical networks.

A modulated signal at 32 Gb/s was used to further test these two switch fabrics, and the experimental setup is shown in Figure 6A. Continuous wave light at 1550.29 nm generated by a tunable laser was launched into the Mach-Zehnder modulator driven by a NRZ-OOK signal (2^{31}-1 pseudo-random binary sequences) from the bit pattern generator. The polarization controller was employed to optimize the polarization state of input signal to maximize the coupling efficiency between fiber and chip. After coupling out of the chip, the processed signal is firstly amplified by the erbium-doped fiber amplifier and then filtered by a band pass filter. The variable optical attenuator is utilized for controlling the power launched into a communication signal analyzer and an error analyzer for eye diagrams and bit error rate (BER) measurements, respectively. For convenience of presentation, here we only show the eye diagrams from port I1 to each output port for the cross-bar switch fabric and ring-bus switch fabric, as shown in Figure 6B. Clean and open eyes were observed for all the paths, indicating a good routing performance of these two switch fabrics. Finally, the BER measurements of the shortest and longest optical paths, i.e. "I1-O1" and "I1-O2" for the cross-bar switch fabric and "I1-O1" and "I1-O4" for the ring-bus switch fabric, are performed, as plotted in Figure 6C and D. For the cross-bar fabric, it can be seen that the maximal power penalty for different optical paths is less than 1 dB, which can be attributed to more MRs involved in the path. For the ring-bus fabric, similar results can be observed. Limited by the experimental facility, the demonstration with simultaneous dual-mode inputting cannot be performed. However, in our opinion, this will not affect the characterization of the proposed scheme. The same characterization method had been utilized by many previous multimode switches [31, 34].

4 Conclusion

In summary, we have proposed general solutions of 2×2 multimode switch, enabling reconfigurable inter-mode and inter-path routing. The switch has a simplified and low-loss design as it can process multiple modes at the same time while avoiding a demultiplexing-processing-multiplexing procedure. Minimum and maximum insertion losses as low as 0.3 and 1.2 dB and low crosstalk of <–16.6 dB for all the channels and switching configurations are experimentally obtained. Two types of switch fabric with cross-bar and ring-bus architectures based on the proposed switch element are fabricated, verifying high feasibility of high-density and large-scale integration. Measured results show a low insertion loss of <3.8 dB and a low crosstalk of <–15 dB. For high-speed communication, 32 Gb/s NRZ-OOK signal transmission is carried out, reaching up to 256 Gb/s of aggregate throughout. The proposed multimode switch can further promote the advanced and flexible MDM optical networks.

Acknowledgments: This work was supported by the National Natural Science Foundation of China (Grant Nos. 61475050 and 61775073), the New Century Excellent Talent Project in Ministry of Education of China (NCET-13-0240) and China Scholarship Council. Reed is the recipient of a Royal Society Wolfson Merit Award and is grateful to both the Royal Society and the Wolfson Foundation for the award. D. J. Thomson acknowledges funding from the Royal Society for his University Research Fellowship.

References

[1] Shacham A, Bergman K, Carloni LP. Photonic networks-on-chip for future generations of chip multiprocessors. IEEE Trans Comput 2008;57:1246–60.
[2] Miller DAB. Device requirements for optical interconnects to silicon chips. Proc IEEE 2009;97:1166–85.
[3] Nagarajan R, Ziari M, Kato M, et al. Large-scale DWDM photonic integrated circuits. In: Optical amplifiers and their applications, Budapest, Optical Society of America, 2005:WA1.
[4] Narasimha A, Analui B, Liang Y, et al. A fully integrated 4×10-Gb/s DWDM optoelectronic transceiver implemented in a standard 0.13 μm CMOS SOI technology. IEEE J Solid-St Circ 2007;42:2736–44.

[5] Doerr C, Chen L, Buhl L, Chen Y. 8-Channel $SiO_2/Si_3N_4/Si/Ge$ CWDM receiver. IEEE Photonic Tech Lett 2011;23:1201–3.
[6] Gill D, Xiong C, Proesel J, Rosenberg J. Demonstration of error free 32 Gb/s operation from monolithic CMOS nano-photonic transmitters. IEEE Photonic Tech Lett 2016;28:1410–3.
[7] Dong P, Lee J, Chen Y, et al. Four-channel 100-Gb/s per channel discrete multitone modulation using silicon photonic integrated circuits. J Lightwave Technol 2016;34:79–84.
[8] Boeuf F, Cremer S, Temporiti E, et al. Recent progress in silicon photonics R&D and manufacturing on 300 mm wafer platform. Optical Fiber Communication Conference, Los Angeles, California, 2015:W3A.1.
[9] Orcutt J, Gill D, Proesel J, et al. Monolithic silicon photonics at 25Gb/s. Optical Fiber Communication Conference, Anaheim, California, 2016:Th4H.1.
[10] van Uden RGH, Correa RA, Lopez EA, et al. Ultra-high-density spatial division multiplexing with a few-mode multicore fibre. Nat Photonics 2014;8:865.
[11] Richardson DJ, Fini JM, Nelson LE. Space-division multiplexing in optical fibres. Nat Photonics 2013;7:354.
[12] Dai D, Wang J, Chen S, Wang S, He S. Monolithically integrated 64-channel silicon hybrid demultiplexer enabling simultaneous wavelength-and mode-division-multiplexing. Laser Photon Rev 2015;9:339.
[13] Shiraishi T, Li Q, Liu Y, et al. A reconfigurable and redundant optically-connected memory system using a silicon photonic switch. Optical Fiber Communication Conference 2014, 2014:1–3.
[14] Sun C, Wade M T, Lee Y, et al. Single-chip microprocessor that communicates directly using light. Nature 2015;528:534–8.
[15] Van Campenhout J, Green WM, Assefa S, Vlasov YA. Low-power, 2×2 silicon electro-optic switch with 110-nm bandwidth for broadband reconfigurable optical networks. Opt Express 2009;17:24020–9.
[16] Dong P, Liao S, Liang H, et al. Submilliwatt, ultrafast and broadband electro-optic silicon switches. Opt Express 2010;18:25225–31.
[17] Chen L, Chen Y-K. Compact, low-loss and low-power 8×8 broadband silicon optical switch. Opt Express 2012;20: 18977–85.
[18] Yang M, Green WM, Assefa S, et al. Non-blocking 4×4 electro-optic silicon switch for on-chip photonic networks. Opt Express 2011;19:47–54.
[19] Han SY, Seok TJ, Quack N, Yoo B-W, Wu MC. Large-scale silicon photonic switches with movable directional couplers. Optica 2015;2:370–5.
[20] Murray K, Lu ZQ, Jayatilleka H, Chrostowski L. Dense dissimilar waveguide routing for highly efficient thermo-optic switches on silicon. Opt Express 2015;23:19575–85.
[21] Chen S, Shi Y, He S, Dai D. Low-loss and broadband 2×2 silicon thermo-optic Mach–Zehnder switch with bent directional couplers. Opt Lett 2016;41:836–9.
[22] Seok TJ, Quack N, Han S, Muller RS, Wu MC. Large-scale broadband digital silicon photonic switches with vertical adiabatic couplers. Optica 2016;3:64–70.
[23] Wilkes CM, Qiang X, Wang J, et al. 60 dB high-extinction auto-configured Mach–Zehnder interferometer. Opt Lett 2016;41:5318–21.
[24] Nikolova D, Calhoun DM, Liu Y, et al. Modular architecture for fully non-blocking silicon photonic switch fabric. Microsyst Nanoeng 2017;3:16071.
[25] Pérez D, Gasulla I, Crudgington L, et al. Multipurpose silicon photonics signal processor core. Nat Commun 2017;8:636.
[26] Seok TJ, Kopp VI, Neugroschl D, Henriksson J, Luo J, Wu M. High density optical packaging of high radix silicon photonic switches. Optical Fiber Communication Conference Postdeadline Papers, Los Angeles, California, 2017:Th5D.7.
[27] Hwang HY, Morrissey P, Lee JS, et al. 128×128 silicon photonic MEMS switch package using glass interposer and pitch reducing fibre array. 2017 IEEE 19th Electronics Packaging Technology Conference (EPTC), Singapore, 2017:1–4.
[28] Wu X, Xu K, Dai D, Tsang HK. Mode division multiplexing switch for on-chip optical interconnects. Opto-Electronics and Communications Conference and Photonics Switch Conference (OECC/PS), Japan, Niigata, 2016:ThE2–4.
[29] Wang S, Wu H, Tsang HK, Dai D. Monolithically integrated reconfigurable add-drop multiplexer for mode-division-multiplexing systems. Opt Lett 2016;41:5298–301.
[30] Wang SP, Feng XL, Gao SM, et al. On-chip reconfigurable optical add-drop multiplexer for hybrid wavelength/mode-division-multiplexing systems. Opt Lett 2017;42:2802–5.
[31] Stern B, Zhu X, Chen C, et al. On-chip mode-division multiplexing switch. Optica 2015;2:530–5.
[32] Zhang Y, Zhu Q, He Y, Qiu C, Su Y, Soref R. Silicon 1×2 mode- and polarization-selective switch. Optical Fiber Communication Conference, Los Angeles, California, 2017:W4E.2.
[33] Jia H, Zhou T, Zhang L, Ding J, Fu X, Yang L. Optical switch compatible with wavelength division multiplexing and mode division multiplexing for photonic networks-on-chip. Opt Express 2017;25:20698–707.
[34] Yang L, Zhou T, Jia H, et al. General architectures for on-chip optical space and mode switching. Optica 2018;5:180–7.
[35] Sun C, Yu Y, Chen G, Zhang X. Integrated switchable mode exchange for reconfigurable mode-multiplexing optical networks. Opt Lett 2016;41:3257–60.
[36] Chan W, Chan H. Reconfigurable two-mode mux/demux device. Opt Express 2014;22:9282–90.
[37] Sun C, Yu Y, Chen G, Zhang X. On-chip switch for reconfigurable mode-multiplexing optical network. Opt Express 2016;24:21722–8.
[38] Huang Q, Jin W, Chiang KS. Broadband mode switch based on a three-dimensional waveguide Mach-Zehnder interferometer. Opt Lett 2017;42:4877–80.
[39] Suzuki K, Tanizawa K, Matsukawa T, et al. Ultra-compact 8×8 strictly-non-blocking Si-wire PILOSS switch. Opt Express 2014;22:3887–94.
[40] Tanizawa K, Suzuki K, Toyama M, et al. Ultra-compact 32×32 strictly-non-blocking Si-wire optical switch with fan-out LGA interposer. Opt Express 2015;23:17599–606.
[41] Ma Y, Zhang Y, Yang S, et al. Ultralow loss single layer submicron silicon waveguide crossing for SOI optical interconnect. Opt Express 2013;21:29374–82.
[42] Wang J, Xuan Y, Qi MH, et al. Broadband and fabrication-tolerant on-chip scalable mode-division multiplexing based on mode-evolution counter-tapered couplers. Opt Lett 2015;40:1956–9.
[43] Suzuki K, Cong G, Tanizawa K, et al. Ultra-high-extinction-ratio 2×2 silicon optical switch with variable splitter. Opt Express 2015;23:9086–92.
[44] Liu K, Zhang C, Mu S, Wang S, Sorger VJ. Two-dimensional design and analysis of trench-coupler based silicon Mach-Zehnder thermo-optic switch. Opt Express 2016;24:15845–53.